Study of the Formation of the Mesoporous Material SBA-15 by EPR Spectroscopy

Sharon Ruthstein,† Veronica Frydman,† Shifra Kababya,† Miron Landau,‡ and Daniella Goldfarb*,†

Department of Chemical Physics, Weizmann Institute of Science, Rehovot, 76100, Israel, and Blechner Center for Applied Catalysis and Process Development, Chemical Engineering Department, Ben-Gurion University of the Negev, Beer-Sheva, 84105, Israel

Received: August 27, 2002; In Final Form: December 2, 2002

SBA-15 is an hexagonal mesoporous material which is synthesized with nonionic poly(ethylene oxide)-poly(propylene oxide)-poly(ethylene oxide) block copolymers (Pluronics, $EO_yPO_xEO_y$), templates. Pore diameters in the range of 2−30 nm can be obtained with a relatively thick silica wall (up to 6 nm). This material possesses both large, uniform, and ordered channels, along with a complementary net of micropores which provides connectivity between the ordered channels through the silica. This study focuses on the investigation of the formation mechanism of SBA-15 with emphasis on the PEO interactions with the silica and the initiation of the micropores. This was achieved using in situ X-band EPR spectroscopy in combination with electron spin−echo envelope modulation (ESEEM) experiments. The paramagnetic centers were introduced as spin-labeled Pluronic L62 ($EO_6PO_{30}EO_6$) where nitroxides replace the OH groups at the end of the polypropylene oxide (PEO) blocks (L62-NO). Initially, the acidic reaction conditions were adjusted to prevent the decomposition of the nitroxide radical, while still producing highly ordered SBA-15. Then, the locations of the nitroxides of L62-NO within the micelles of Pluronic P123 ($y = 20$, $x = 70$) and L64 ($y = 13$, $x = 30$) were determined through three-pulse ESEEM experiments on solutions prepared in D_2O. In these experiments, the ^2H modulation induced by D_2O was compared with that of a series of small spin-probes with known hydrophilic and hydrophobic characters that were introduced into the micelles. The NO group of L62-NO was found to be close to the core-corona interface in both types of Pluronics. The temporal evolution of the EPR spectrum during the reaction showed that for SBA-15 made with P123 the most significant changes in the L62-NO spectrum occur within the first 100 min. Furthermore, X-ray diffraction measurements of dried materials showed that the hexagonal structure of SBA-15 is also created within the first 2 h. A partitioning of the L62-NO between the precursors of the mesopores and micropores of the SBA-15 structure takes place at the very early stages of the reaction, and a continuous depletion of water within the corona−core interface was observed. In the final product obtained without a thermal stage, the majority of the PEO chains are located in the micropores. The extent of the PEO chains located within the silica micropores depends on the thermal stage temperature and on the Si/P123 molar ratio. In the L64 synthesis, practically all of the NO groups of L62-NO are located within the silica network and experience a single environment.

Introduction

Since the discovery of the M41S mesoporous materials in 1992,[1,2] there has been an increasing interest in the design of novel porous materials tailored with various pore organization and dimensions for potential applications in separation, catalysis, chemical sensing, and low dielectric and optical coating.[3] The synthesis process of mesoporous materials involves the formation of organic−inorganic composites by a self-assembly process, where the organic phase is organized on a mesoscopic scale and serves as a template for the inorganic skeleton. Different mesostructures and pore sizes can obtained by adjusting the synthesis conditions and the nature of the surfactant. Silica materials exhibiting lamellar, 2D hexagonal, 3D hexagonal, or cubic organizations, with pores in the range of 1.5−4.0 nm, have been produced with ionic surfactants such as alkyltrimethylammonium bromide or chloride, or double headed gemini quaternary ammonium salts, with various alkyl chain lengths.[1,2,4,5,7]

Mesoporous materials with larger pore sizes and better stability as compared to the M41S materials were recently synthesized with nonionic poly(ethylene oxide)-poly(propylene oxide)-poly(ethylene oxide) block copolymers (Pluronic, $EO_yPO_xEO_y$).[8] In these materials, the pore diameter can be tuned within the range of 2−30 nm, and its better stability stems from its thicker silica wall (up to 6 nm). The use of block copolymers in the synthesis of ordered inorganic porous matrices is one of the most promising routes in terms of high degree of ordering, low cost, and low toxicity. The polymer template can be readily removed by extraction or calcination, and the resulting material has a very good hydrothermal stability.[8]

The formation mechanism of mesoporous materials is complicated and not fully understood. It involves specific interactions between the organic template and inorganic precursors that eventually result in a long-range structural order. Understanding the details of the formation mechanism of mesoporous materials should allow to predict and control the properties of the final products. The driving force for the interaction between the organic aggregates and the inorganic precursors in the case of charged surfactants is electrostatic and several schemes have

* To whom correspondence should be addressed.
† Weizmann Institute of Science.
‡ Ben-Gurion University of the Negev.

10.1021/jp021964a CCC: $25.00
Published on Web 02/01/2003

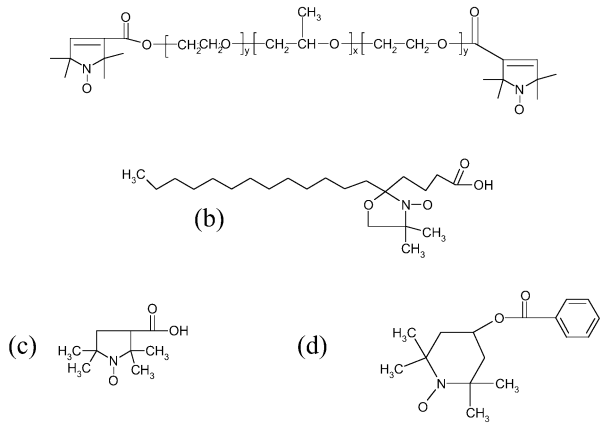

Figure 1. Spin probes used in this study: (a) L62-NO, (b) 5DSA, (c) 3-carboxy-proxyl, and (d) 4-hydroxy-tempo-benzoate.

been suggested by Monnier et al.[9] Tanev and Pinnavaia[10,11] showed that the assembly of mesoporous materials can also be driven by hydrogen bonds in the case of neutral templates such as nonionic poly(ethylene oxide) (PEO) surfactants and inorganic precursors. Zhao et al.[8] proposed that the formation of SBA-15 occurs through a scheme where the silica source is first hydrolyzed at low pH to form $Si(OMe)_{4-n}(OH_2^+)_n$ species and the PEO moieties of the block copolymer associate with hydronium ions. Then, the charged PEO units and the cationic silica species are assembled together, via Cl^-, by a combination of electrostatic, hydrogen bonding and van der Waals interactions.

One of the interesting properties of SBA-15 is the coexistence of meso- and micropores. This was first noted by Ryoo et al.,[12] who found that the structure of SBA-15 synthesized with Pluronic P123 ($EO_{20}PO_{70}EO_{20}$) consists not only of large, uniform, and ordered channels but also of much smaller complementary pores which provide connectivities between the ordered mesochannels. These pores appear to be stable up to 900 °C, but calcination at 1000 °C eliminates them. Galarneau et al.[13] showed that when the synthesis temperature increases from 35 to 130 °C the wall thickness of SBA-15 decreases from 40 to 20 Å, and at 130 °C, almost no complementary pores are present. Similar results were reported by Imperor-Clerc et al.[14] It was also observed that the Si/polymer ratio in the starting gel affects the extent of the micropores in the silica network,[15,16] at higher Si/P123 ratio, the degree of the microporosity increases. The source of the microporosity has been ascribed to PEO chains that are trapped within the silica region during the synthesis and are removed by calcination, leaving open micropores.[17] Melosh et al.[18] showed by NMR of mesoscopically ordered silica, formed with 50 wt % Pluronic F127 ($EO_{106}PO_{70}EO_{106}$), that the methylenes in the PEO chains are closer to the silica network than those of the polypropylene (PPO) block. Furthermore, there was a large difference in the mobilities of the PEO chains and the PPO block, the latter being significantly more mobile. There are no reports, however, on the partition of the PEO chains within the micropores and the mesopores and on the details of the micropore formation.

Here we present an in situ investigation of the formation mechanism of SBA-15, along with the examination of its final internal surface properties and pore structure. This is carried out primarily through EPR spectroscopy of spin-probes with emphasis on the PEO interaction with the silica and the initiation of the micropores. The methods are similar to those applied earlier in the investigation of the formation mechanism of MCM-41.[19−21] The spin probe used is L62-NO (Figure 1), which is also a block copolymer (Pluronic L62, $EO_6PO_{30}EO_6$) where the nitroxides replace the OH groups at the end of the PEO chain. Caragheorgheopol et al.[22] have studied the motional characteristics of L62-NO in micelles of Pluronic P85 ($EO_{27}PO_{39}EO_{27}$) using X-band EPR spectroscopy and reported that L62-NO is indeed incorporated in the micelles and the nitroxide group is situated within the PEO region. This suggests that this spin-probe is an excellent candidate for the investigation of the formation of SBA-15.

Experimental Section

Synthesis. The reagents used for the synthesis were Pluronic P123 ($EO_{20}PO_{70}EO_{20}$, $M_{av} = 5800$), a gift from BASF Corp. (USA), Pluronic L64 ($EO_{13}PO_{30}EO_{13}$, $M_{av} = 2900$; Aldrich), tetramethyl-orthosilicate $(CH_3O)_4Si$ (98%,TMOS, Merck), and *ortho*-phosphoric acid (85% H_3PO_4, Fluka). The spin-probes employed in this study were 4-hydroxy-tempo-benzoate(Aldrich), 3-carboxy-proxyl (Aldrich), and 5-doxyl-stearic-acid (5-DSA, Aldrich; see Figure 1). The spin probe L62-NO was synthesized as described in the literature.[22]

SBA-15 was synthesized according to the procedure reported by Zhao et al.,[23] except for the addition of the spin-probe and the use of *ortho*-phosphoric acid instead of hydrochloric acid. A typical SBA-15 synthesis was as follows: To a 16 mL aqueous solution containing 0.5 g of P123 (86.2 μmol) 20 μmol spin-probe (L62-NO or others) were added at 50 °C, and the mixture was stirred for several minutes until all the spin-probe dissolved. Then, 1.2 mL of H_3PO_4 85% (12 mmol) were added, the mixture was stirred for two more minutes, followed by the addition of 0.8 mL (5 mmol) of TMOS. The resulting mixture was left under stirring for 20 h at 50 °C. Then, half of the gel solution was filtered and dried at ambient temperatures, and the other half was transferred into a Teflon bottle and was heated at 100 °C for 24 h without stirring. After cooling to room temperature, the solid product of both halves was recovered by filtering, washed with distilled water, and dried in air at an ambient temperature. The molar composition of the synthesis gel was as follows: 1 TMOS; 1.7×10^{-2} P123; 2.4 H_3PO_4; 175 H_2O; 4×10^{-3} spin probe. SBA material was also synthesized with L64 using the same procedure and the composition of the synthesis gel was 1 TMOS; 6.8×10^{-2} L64; 2.4 H_3PO_4; 175 H_2O; 4×10^{-3} spin-probe. Samples synthesized at 50 °C, and those that were further heated to 100 °C were calcined at 600 °C.

Spectroscopic Measurements. EPR spectra were recorded on a BRUKER ER200D-SRC spectrometer operating at 9−9.5 GHz. Gel and liquid samples were measured in flat cells and solid samples in 4 mm o.d. quartz tubes. In situ EPR measurements were carried out as follows: A reaction mixture without TMOS and H_3PO_4 was first prepared, and then H_3PO_4 was added under stirring during 2 min, followed by addition of TMOS under vigorous stirring for about 2 more minutes. Part of the mixture was then quickly transferred into an EPR flat cell which was kept in the measuring cavity until the end of the measurement at 50 °C. The solid formed during the experiment remained within the active part of the cavity throughout the measuring period. W-band CW-EPR measurements were carried out on a home-built spectrometer operating at 94.9 GHz.[24]

Electron spin−echo envelope modulation (ESEEM) experiments were carried out on a 9 GHz home-built pulsed EPR spectrometer,[25] and 3 mm o.d. quartz tubes were used. The three-pulse ESEEM sequence, $\pi/2-\tau-\pi/2-T-\pi/2-\tau-$echo, was employed with a four step phase cycling.[26] The $\pi/2$ pulse length was 20 ns, and τ was set to 250 ns. The modulation depth was

taken as $k = a/(a + b)$ where $a + b$ is the interpolated echo intensity between the first and second maxima and b is the echo intensity at the first minimum as shown in Figure 4.

^{13}C solid-state NMR spectra were recorded on a 300 MHz Bruker spectrometer at a frequency of 75.47 MHz. A BL 4 mm Bruker MAS probe was employed at a spinning speed of 10 kHz and the $\pi/2$ pulse duration was 5 μs. ^{13}C cross-polarization magic angle spinning (CPMAS) spectra were acquired under Hartman-Hahn conditions. The RF power was set to 50 kHz with contact time duration of 0.1−5 ms. In addition,^{13}C spectra were measured using the chemical shift echo (CSE) sequence ($\tau = 200$ μs). High power proton decoupling was employed using the TPPM scheme and repetition delays of 3 s (CSE) and 1s (CP) were employed. Up to 4000 transients were averaged, and the ^{13}C chemical shift scale was referenced to TMS.

Small-angle X-ray (SAX) diffraction measurements on dried products were carried out on a SAX diffractometer, equipped with a Franks mirror and one-dimensional position sensitive detector (homemade), using Cu Kα (1.54 Å) with a Ni filter.[27] Surface areas and pore size distributions were obtained from Nitrogen adsorption−desorption isotherms measured at 77 K with a NOVA-2000 (Quantachrome, version 7.11) instrument using conventional BET and BJH methods. The micropores surface area was derived from *t*-plot analysis of the adsorption isotherms. The samples were outgassed under a vacuum at 250 °C.

Spectral Simulation. EPR spectra were simulated using the NLSL program developed by Budil et al.,[28,29] where the dynamic parameters characterizing the molecular motion were obtained by a nonlinear-least-squares fit of the experimental spectrum to model calculation based on the Stochastic Liouville equation. We have used a Brownian diffusion model and an axially symmetric rotational diffusion tensor, thus defining two rate constants $R_{\|}$ and $R_{\perp}$. The simulations require the principal components of the g and A tensors. The principal g-values of L62-NO were determined from the powder pattern recorded at W-band and 50 K using a Mn/MgO standard, yielding $g_{xx} = 2.0069$, $g_{yy} = 2.0052$, and $g_{zz} = 2.0000$. The A values were obtained by fitting the X-band rigid limit spectrum[30] and not using literature values because the hyperfine coupling depends on the local polarity.[31] Using the above g-values, we obtained $A_{xx} = A_{yy} = 5.0$ G and $A_{zz} = 37.2$ G for the spectrum of SBA-15 (L62-NO) recorded at 180 K. The same g- and A-values were used in the simulation of spectra with two species because the changes in the local polarity is negligible compared to the variations in their rotational diffusion rates and order parameter.

Results

Synthesis of SBA-15 with H_3PO_4. The synthesis of SBA-15 is usually carried out in a highly acidic medium. This poses a serious problem when nitroxyl radicals are present because at low pH the radical transforms into a diamagnetic hydroxylamine.[32] Indeed, when the reaction was carried out according to the procedures described in the literature (pH < 1) using concentrated hydrochloric acid,[23] the final product did not show any signal because of the transformation of the radical. To overcome the problem of the spin-probe stability, the hydrochloric acid was replaced with *ortho*-phosphoric acid, which is a milder acid, and most of the spin-label survived the reaction. Figure 2a,b shows the SAX diffractions patterns of as-synthesized and calcined SBA-15 (Si/P123 = 59, 118) obtained after the 100 °C hydrothermal stage prepared with H_3PO_4 as compared to SBA-15 prepared with HCl. The diffraction patterns are typical for the hexagonal structure,[23] and the *d* -values are listed in Table 1. SAX diffraction patterns of SBA-15(Si/P123 = 59) (obtained without the hydrothermal thermal stage are similar, and examples are presented in Figure 2c. Nitrogen absorption measurements carried out on the calcined materials exhibit the typical adsorption−desorption isotherms[17] as shown in Figure 3. Table 1 summarized these results, listing the total surface area, the relative micropores surface area, and the average pore sizes of the samples investigated. The use of H_3PO_4 increased the reaction time but did not affect the structure of the final product. Stucky and co-workers[8] showed that the

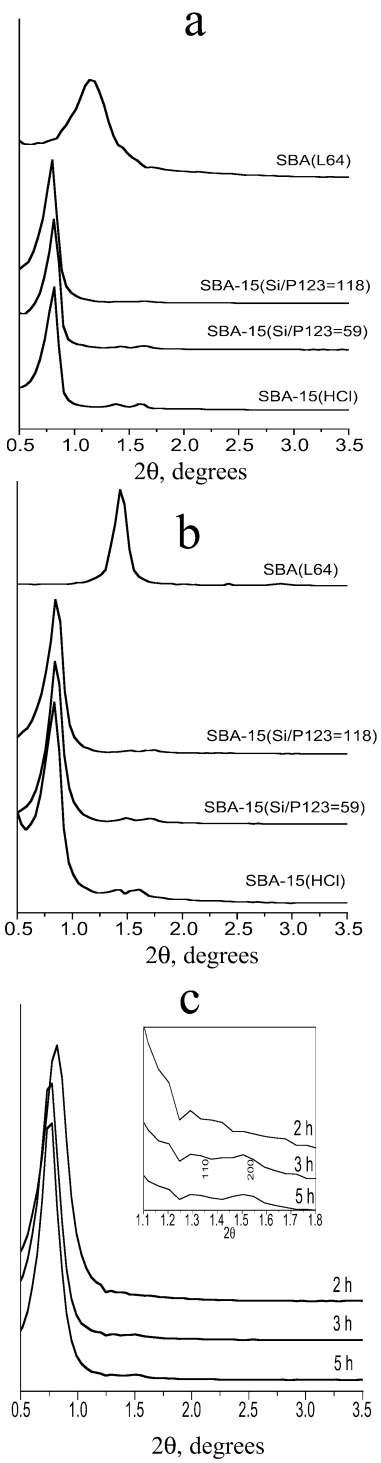

Figure 2. (a) SAX powder diffraction patterns of as-synthesized SBA-15(P123) synthesized with HCl and H_3PO_4 and of SBA(L64) synthesized with H_3PO_4 (after thermal stage at 100 °C). (b) Same as part (a) after calcination. (c) SAX powder diffraction patterns of as-synthesized SBA-15(Si/P123 = 59) synthesized with H_3PO_4 at 50 °C for 2, 3, and 5 h.

TABLE 1: Summary of the SAX Diffraction and Nitrogen Absorption Results of the SBA Materials Prepared

sample	d-spacing[a] (Å)	total surface area (m^2/g)	% micro-porosity surface area	average pore size diameter (Å)
Si/P123 = 59, 50 °C	108 (92)	609	51	40
Si/P123 = 59, 100 °C	110 (103)	900	48	40[b]
Si/P123 = 118, 50 °C	108 (92)	583	68	33
Si/P123 = 118, 100 °C	110 (103)	851	48	39.5
Si/L64 = 15, 100 °C	77.3 (64.1)	975	36	45

[a] Determined from SAX diffraction. The number in brackets corresponds to the calcined materials. [b] The pore size distributions showed two peaks at 37 and 52 Å.

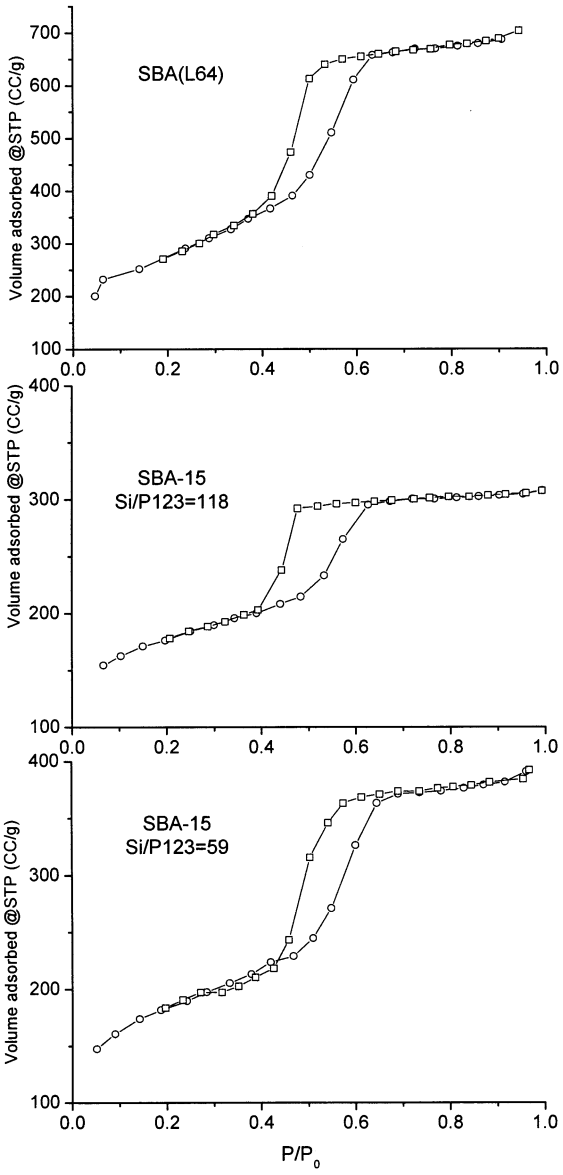

Figure 3. Nitrogen adsorption isotherms of (bottom) SBA-15 prepared with H_3PO_4, Si/P123 = 59 at 50 °C, (middle) same with Si/P123 = 118, (top) SBA prepared with L64 after thermal stage, 100 °C.

time required for the silica precipitation in the synthesis of SBA with the nonionic PEO surfactant − Triton X-100 depends on $[H^+]$ and the anion used. The trend in the precipitation time was found to be HBr ∼ HCl < HI < HNO_3 < H_2SO_4 ≪ H_3PO_4.

Mesoporous SBA was also prepared with L64 and H_3PO_4 (SBA(L64)). The SAX diffraction pattern of SBA(L64) synthesized without the hydrothermal stage showed a broad peak indicating poor ordering. The hydrothermal stage improved the order significantly as shown in Figure 2a, and calcination resulted in additional improvement (Figure 2b). There, the *d*-spacing is smaller than in the materials prepared with P123 as expected because of the shorter polymeric chains. The nitrogen adsorption isotherms presented in Figure 3 show that the material is mesoporous, and Table 1 lists its surface area characteristics: high surface area and a relatively low degree of microporosity compared to the material prepared with P123.

Location of the Spin Probe. At 50 °C, a water solution of 2.5 wt % P123 consists of spherical micelles in which two regions were identified.[33] The first is the corona of the micelles which comprises mostly the PEO chains, and the second is its core, containing the PPO chains.[34] Because the spin-probe senses changes occurring in its close environment, it is essential to determine its location within the initial micellar structure. This can be obtained by ESEEM spectroscopy, which is highly effective for measuring the weak superhyperfine interactions of an electron spin with nearby nuclear spins.[35,36] In ESEEM measurements, a series of microwave (MW) pulses generates an echo, and the echo decay is followed as a function of one of the time intervals between the pulses. When an anisotropic hyperfine interaction is present, the echo decay exhibits modulation, the depth (k) of which is a function of the electron−nuclear distance, the number of nuclei, and their nuclear spin.[37] Kevan and co-workers have extensively applied ESEEM methods to study a variety of photoionization and charge separation problems in micellar and vesicular systems.[38−41] In addition, they have determined the location of nitroxide spin-probes in micelles by following the interaction of the nitroxide group with specifically deuterated surfactant molecules.[42,43] We have recently adopted this approach and applied it to investigate the formation of MCM-41.[44] Here we use it to estimate the position of the nitroxide of L62-NO within the P123 micelles by comparing the ^{2}H modulation depth, $k(^2H)$, of the ESEEM traces of four different spin-probes dissolved in 2.5 wt % P123 solutions in D_2O. In this set of experiments, a deeper ^{2}H modulation corresponds to a higher exposure to D_2O. The ESEEM experiments are best performed at low temperatures where molecular motions that average the anisotropic hyperfine interaction have been frozen out and where relaxation times are long enough to allow echo detection. Accordingly, solutions that were kept at 50 °C were rapidly quenched by insertion into liquid nitrogen. It has already been shown that such a rapid cooling conserves the micellar structure.[30,44]

Figure 4a presents the $k(^2H)$ of a 1 mM L62-NO solution in D_2O compared with 1 mM L62-NO, 3-carboxy-proxyl, 5DSA, and 4-hydroxy-tempo-benzoate in 2.5 wt % P123 solutions in D_2O. The concentration of P123 is the same as that used in the synthesis of SBA-15. The largest $k(^2H)$ value is observed for L62-NO in D_2O because in this system there are no micelles and the spin-label is surrounded by water molecules. When micelles are present, $k(^2H)$ depends on the location of the spin-label within the micelles. For instance, $k(^2H)$ of a spin-label that is located in the core of the micelles (PPO region) should be smaller than that of a spin-label situated in the corona of the micelles (PEO region). The spin-probe 3-carboxy-proxyl exhibits the largest $k(^2H)$ within the series. It is small, hydrophilic, and water soluble, and therefore, it is located at the region of the water/micelle interface. The spin-probe 4-hydroxy-tempo-benzoate exhibits the lowest $k(^2H)$ values because it is hydrophobic and located within the core of the micelle. 5DSA is water insoluble and consequently must be dissolved in the micelle,

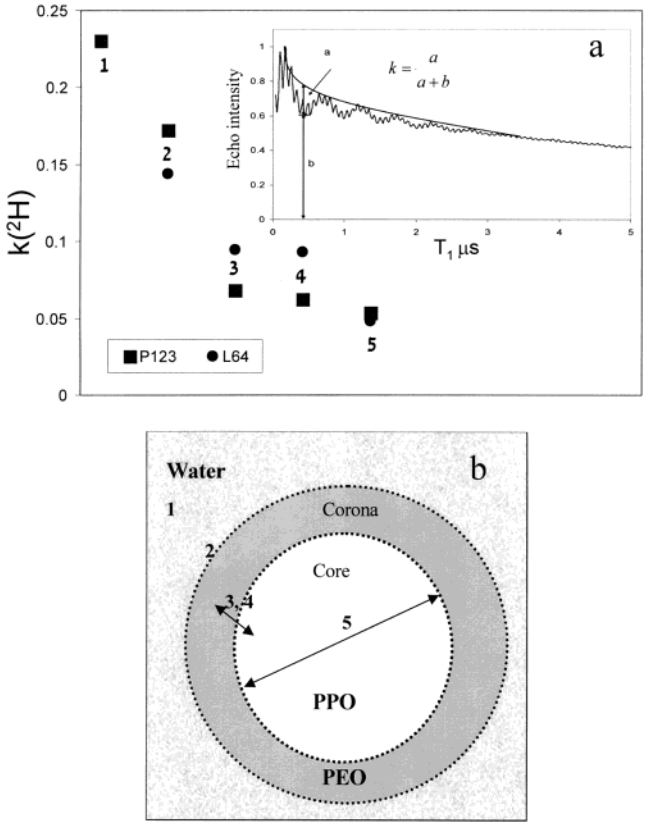

Figure 4. (a) $k(^2H)$ of 1 mM L62-NO in D_2O (1) and 1 mM 3-carboxy-proxyl (2), 5DSA (3), L62-NO (4), and 4-hydroxy-tempo-benzoate (5) in a solution of 2.5 wt % P123 + D_2O (■) or 5 wt % L64 + D_2O (●). (b) A schematic description of the micelles and the location of the different spin-probes.

but, because of its polar headgroup, the spin-label should be located in the core−corona interface region. This is indeed observed experimentally, the $k(^2H)$ of 5DSA is higher than that of 4-hydroxy-tempo-benzoate and lower than that of 3-carboxy-proxyl. Finally, the $k(^2H)$ of L62-NO is slightly smaller than that of 5DSA, placing it closer to the core. L62 has shorter PPO and PEO blocks than P123, and therefore, the ends of its PEO chains are situated well inside the corona, closer to the core. Figure 4b depicts the estimated location of the different nitroxide spin-labels in the micelle as obtained from the ESEEM experiments. For comparison, we have also measured the ESEEM of the various spin-probes in a solution of 5 wt % L64, which has shorter PEO and PPO blocks ($EO_{13}PO_{30}EO_{13}$) (see Figure 4a). The L64 concentration used is similar to that employed in the SBA(L64) synthesis. The trend observed was similar to that of the P123 solutions, with the exception that the $k(^2H)$ of L62-NO and 5DSA are larger in L64 than in P123 due to the shorter PEO chains of L64.

Temperature Effect on Micellization. The critical micelle concentration (CMC) of P123 exhibits an unusual temperature dependence; it decreases with increasing temperature.[33] For example, it is 4.5 wt % at 17 °C and 3×10^{-4} wt % at 43 °C.[34] The effect of temperature on micellization of a 10 wt % aqueous solution of P85 was investigated by EPR of L62-NO,[22] but the effect of the pH has not been explored. Because the formation of SBA-15 requires a low pH,[8] we have investigated the micellization of a 2.5wt % aqueous solution of P123 at the reaction temperature with and without acid to establish the organization of the P123 prior to the addition of the silica source. Figure 5a shows the temperature dependence of the EPR spectrum of 1 mM L62-NO in a 2.5 wt % P123 aqueous solution

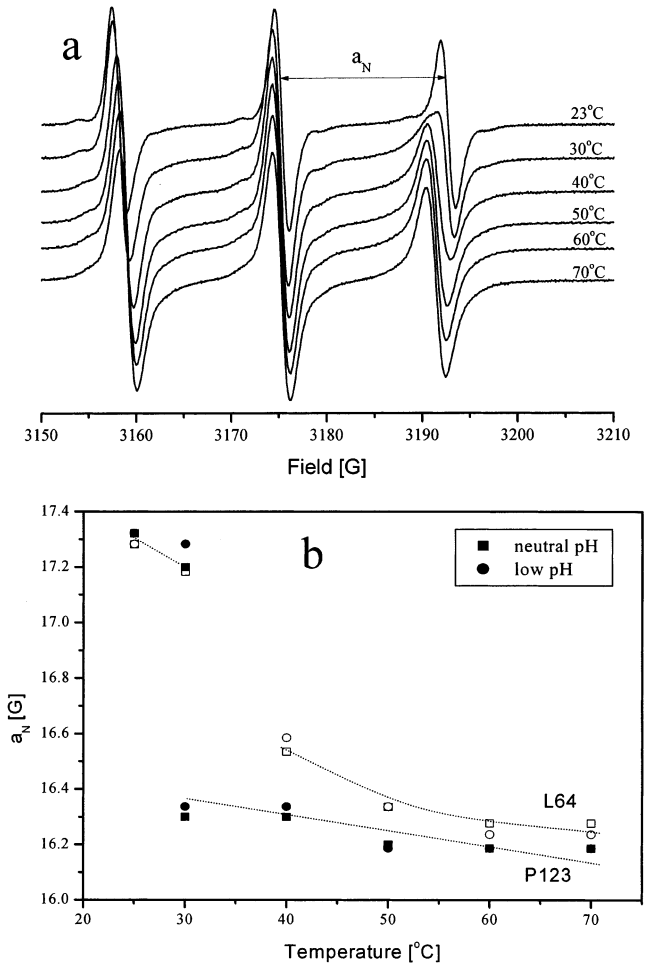

Figure 5. (a) Temperature dependence of the EPR spectrum of L62-NO in 2.5 wt % aqueous solution of P123 at neutral pH. (b) The temperature dependence of the ^{14}N hyperfine coupling (a_N) of L62-NO in 2.5 wt % aqueous solution of P123 (filled symbols) and in 5 wt % L64 (empty symbols) aqueous solution at neutral pH and low pH. The dotted lines were drawn to guide the eye.

at a neutral pH. The spectrum recorded at 23 °C shows a triplet due to the hyperfine interaction of ^{14}N with $a_N = 17.3$ G corresponding to L62-NO in water. The 30 °C spectrum exhibits a splitting in the high field hyperfine components, indicating a superposition of two spectra, one with a_N similar to that observed at 23 °C and the other with $a_N = 16.3$ G, attributed to L62-NO in the micelles. At 40 °C, the spectrum exhibits a single triplet with $a_N = 16.3$ G indicating that all of the spin-probe is now located within the micelles. The temperature dependence of a_N is summarized in Figure 5b. The decrease in the a_N value indicates a reduction in the polarity of the environment, consistent with L62-NO located in the micelles.[22] Upon further increase in the temperature, the a_N value no longer changes and the line narrows due to the increase in the rotational diffusion rate. The temperature dependence of the EPR spectrum of a similar solution but at pH = 1.3 obtained by the addition of H_3PO_4 was similar, and the a_N behavior is summarized in Figure 5b as well. The same dependence at neutral and acidic pH indicates that H_3PO_4 has no influence on the micellization.

Temperature dependence measurements (at neutral and pH = 1.3) were carried out also on L62-NO in a 5 wt % L64 solution, and the changes in the a_N values are presented in Figure 5b. Here too, the addition of H_3PO_4 did not affect the micellization process. The curve obtained is in general similar to that of P123, showing the formation of micelles above 40

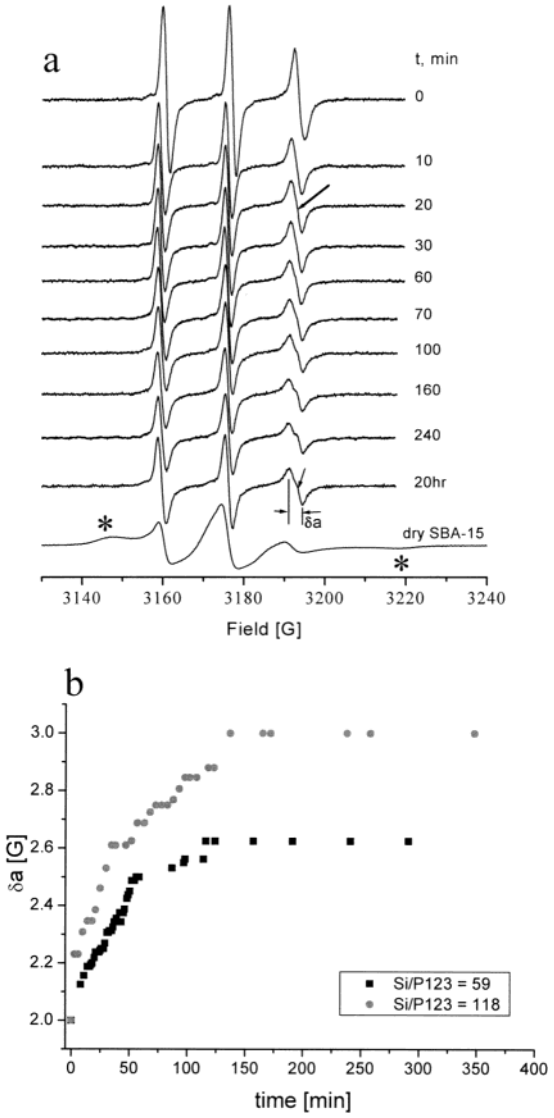

Figure 6. (a) Time evolution of the EPR spectrum of L62-NO during the formation of SBA-15 (Si/P123 = 59) at 50 °C and of the dry product recorded at room temperature. The spectral features of the immobilized species are marked by *. (b) The time evolution of δa during the formation of SBA-15 at 50 °C for Si/P123 molar ratios of 59 and 118.

°C although the a_N is somewhat larger. This indicates a more polar environment for the spin-label in L64 micelles, as expected considering the shorter PEO chains of L64. This is also consistent with the ESEEM results described above.

In Situ EPR Measurements. Once the location of L62-NO in the initial micelles has been determined and the pH effect established, we proceeded to the in situ EPR investigation of the formation of SBA-15(P123). The spectra recorded at 50 °C are shown in Figure 6a where $t = 0$ corresponds to the TMOS addition. The spectrum marked with $t = 0$ was recorded before the TMOS addition. During the first 20 min, the spectrum is characteristic of a single species; thereafter, a detectable splitting in the high field component, denoted by δa, indicates the appearance of a second species. The reduction in the total intensity of the spectrum with increasing reaction time is due to partial decomposition of the spin-label at low pH. The time evolution of δa, obtained by acquiring the spectrum only in the region of the high field hyperfine component is presented in Figure 6b. It shows that the major reorganization occurs during the first 2 h, thus suggesting that the structure of SBA-15 is generated within this time, and thereafter, only minor changes

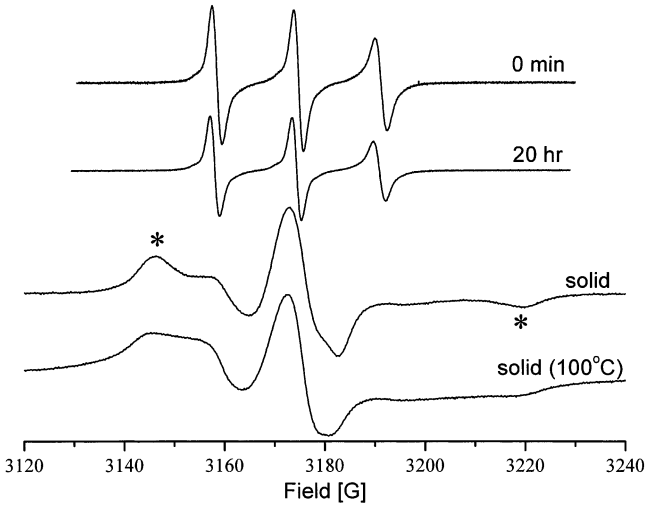

Figure 7. EPR spectra of L62-NO in the reaction mixture of SBA-15(L64) at $t = 0$ min and $t = 20$ h at 50 °C and of the dry solids obtained without and with the 100 °C thermal stage, recorded at room temperature.

that are not detected by the EPR spectrum occur. This is confirmed by the SAX patterns of the dried solids obtained after 2, 3, and 5 h, shown Figure 2c. They all show that indeed an hexagonal structure is created within the first 2 h, but there is a change in the *d*-spacing of the 100 plane from 102.6 Å after 2 h to 108.0 Å after 5 h. The time evolution of δa was also followed for the reaction mixture of SBA-15 with a higher silica content, Si/P123 = 118 as shown in Figure 6b. There, it takes somewhat longer to reach the final values (~150 min) of δa. Moreover, the final δa value is larger.

In principle, the resolution of the high field component of the two species can arise from differences in line width caused by different mobilities. Alternatively, it can be due to a shift of one of the components because of combined changes in g and a_N. Simulations of the composite high field component showed that it can be best reproduced using a superposition of two Lorentzian lines, where the position of one changes with time while the width remains practically constant. In the case of Si/P123 = 59, the change in position amounts to a reduction of a_N by ~1.7 G, whereas for Si/P123 = 118, it is ~2.1 G. These simulations showed that a small decrease in the relative intensity of the component with the decreasing a_N (~20%) occurs. The final relative amount (prior to drying) of this component was 50% and 60% for Si/P123 values of 59 and 118, respectively.

The triplet EPR spectra measured throughout the reaction (Figure 6a) show that the spin-label in both locations is highly mobile (on the EPR time scale) as long as it has not been dried. After filtering and drying at ambient temperatures, one of the species remained fairly mobile, whereas the other exhibited a characteristic rigid limit powder pattern (marked with * in the bottom trace of Figure 6a). Although in the reaction with P123 the presence of a second L62-NO environment became evident already after 20 min, with L64, the spectrum of L62-NO showed a single triplet that remained invariant throughout the reaction as shown in Figure 7. The spectrum obtained after filtering and drying (prior to the thermal stage, see below) is characteristic of a single, highly immobile species (see Figure 7).

Effect of the Reaction Temperature. The synthesis of SBA-15 is usually carried out in two stages. The first one takes place at 50 °C and was described above. The second stage involves a thermal treatment where the aged gel is transferred into a Teflon bottle and heated for 24 h. The effect of this stage is described in this section. The reaction mixture which underwent

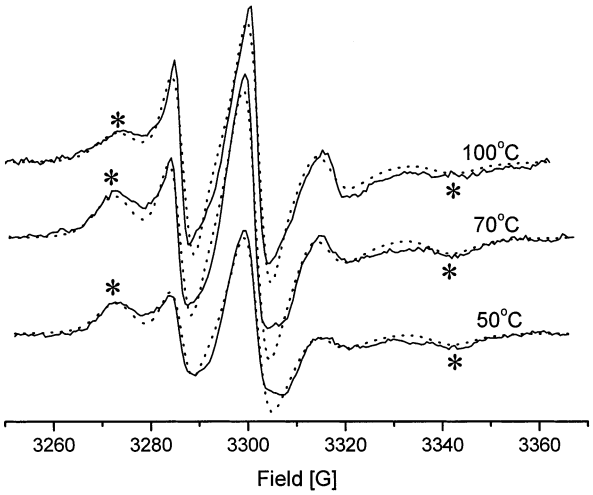

Figure 8. Room-temperature EPR spectra of L62-NO in SBA-15(P123) as a function of the temperature of the thermal stage (solid traces) and best fit simulated EPR spectra (dotted traces). The spectral features of the immobilized species are marked by *. The spectrum labeled with 50 °C was obtained from a sample dried prior to the thermal stage.

TABLE 2: Best-Fit Parameters Used in the Simulations Shown in Figure 8

	mobile species	immobile species
β (tilt angle)	10°	10°
$R_\perp$	1.0×10^8 s^{-1}	1.0×10^7 s^{-1}
$R_\parallel$	1.6×10^8 s^{-1}	2.0×10^5 s^{-1}
line width	3.0 G	6.5 G

the first stage (50 °C, 24 h) was divided into four parts. One was filtered immediately and dried in air at room temperature, whereas the other samples were heated to 70, 100, and 120 °C for 24 h only and then was the solid recovered by filtration and dried at room temperature. The spectra of the 50, 70, and 100 °C samples are presented in Figure 8. The spectrum of the sample heated to 120 °C did not show a signal indicating that the spin-probe decomposed at this temperature. The three spectra are typical of a superposition of two species, one highly mobile and the other immobilized, but they differ in the relative amounts of the two species. As the temperatures of the hydrothermal stage increase, a decrease in the relative intensity of the immobile species (marked with * on the Figure) takes place.

The relative amounts of the two species in the three samples were determined using simulations represented by dotted traces in Figure 8, and the best fit parameters are listed in Table 2. The amount of the mobile species after a reaction at 50 °C is 23%, it increases to 28% at 70 °C, and finally it reaches 40% at 100 °C. The thermal stage also leads to an increase in the *d*-value (see Table 1) similar to the results of Zhao et al.[45] When increasing the molar ratio of Si/P123 by a factor of 2 (from 59 to 118) a decrease of 50% in the relative amount of the mobile species was noticed. The effect of the thermal stage on the spectrum of L62-NO in SBA(L64) is shown in Figure 7. The line shape change is manifested mainly in the broadening of the A_{zz} features, clearly indicating an increase in the mobility.

Information regarding the chain mobility in the final product was also obtained from ^{13}C MAS NMR. The ^{13}C chemical shift echo (CSE) and cross polarization (CP) solid state MAS NMR spectra of SBA-15(P123) synthesized at 50 °C without the thermal stage are shown in Figure 9a. The spectra show three narrow signals similar to those observed earlier by Melosh et al.[18] The 17 ppm peak is due to the methyl group in the PPO chains, and the 74 and 76 ppm signals are due the CH and CH_2 of the PPO chains. Comparison of the CPMAS spectra recorded

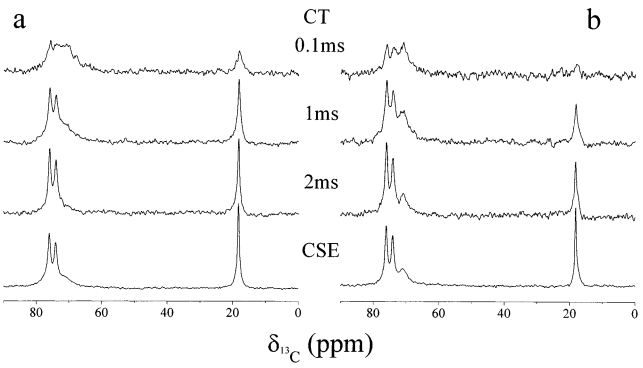

Figure 9. ^{13}C MAS NMR spectra of SBA-15(P123) synthesized at 50 °C without (a) and with the 100 °C thermal stage (b). The top three traces represent CPMAS spectra recorded with different contact time (CT), as noted on the figure, and the bottom trace is the chemical shift echo spectrum obtained after direct excitation of ^{13}C and a spinning speed of 5 kHz.

with different contact times reveals an additional broad signal centered about 73 ppm corresponding to the CH_2 in the PEO block. This signal is best observed at short contact times. Although the relative intensities in the CPMAS spectra cannot be interpreted quantitatively, those measured using the chemical shift echo (CSE) experiment can. The expected relative intensity of the CH_2 lines of PPO and PEO is 7:8. Indeed, deconvolution of the bottom spectrum of Figure 9a, measured using CSE, yields a similar ratio confirming the assignment of the broad peak to PEO. Application of the CPMAS echo sequence with an increasing time interval between the pulses did not reveal a difference in line width of the PEO peak indicating that the broadening is inhomogeneous. This implies the presence of heterogeneity in the environment of the PEO chains. CPMAS spectra measured with different contact time (see Figure 9a) show that as the contact time increases, the narrow PPO peaks become dominant, and the broad PEO signal disappears. This indicates that the ^{13}C of the PPO chains have a longer rotating-frame-relaxation time, $T_{1\rho}$, compared to the PEO nuclei and are therefore more mobile.[18] The spectra shown in Figure 9b are of as-synthesized SBA-15(P123) after the thermal stage, recorded under the same conditions as those of the samples obtained after the first synthesis stage only. The major difference between the two sets is the appearance of a narrow line at 72 ppm, attributed to the PEO chains. This shows that part of the PEO chains experience a more homogeneous environment. Moreover, their $T_{1\rho}$ becomes more similar to those of the PPO carbons, indicating increased mobility as well (on the NMR time scale).

Discussion

The incorporation of the spin-labeled block copolymer L62-NO into the reaction mixture of SBA-15(P123) and SBA(L64) allowed us to follow the reaction kinetics and to provide new insight into the formation mechanism. Both the ESEEM experiments and the temperature dependence of a_N showed that before the initiation of the reaction the nitroxide radical of L62-NO is located in the inner part of the corona of the P123 micelles. The decrease in a_N with the formation of micelles indicates that the environment of the spin-label became less polar, which is consistent with a reduction in the water content and the hydration value.[46] L62-NO has the same general structure as P123, and therefore the PPO block of L62-NO is expected to be intercalated in the PPO core with the NO radical localized in the PEO shell. However, because the PEO length

of L62-NO is significantly shorter than that of P123 (6 vs 20), its chain end with the nitroxide group is closer to the corona−core interface than to the water interface. This observation is substantiated by the similar modulation depth of 5DSA and L62-NO and the increased k(^{2}H) of L62-NO in the L64 micelles.

The NO group of L62-NO in as-synthesized SBA-15 prepared with P123 is partitioned between two environments. In one, the spin-label is highly mobile, whereas in the other it is immobilized (on the EPR time scale). On the basis of these dynamic characteristics, we attribute the two environments to the mesopores and micropores of the SBA-15 structure.[12] The mobile end chains are located within the organic part, whereas the immobilized L62-NO PEO chains are located within the micropores, where their motion is highly hindered. This assignment is supported by the reduction in the relative amount of the mobile species in the samples prepared with the higher Si/P123 which have higher degree of microporosity (see Table 1).[16] Moreover, EPR spectra of SBA-15 obtained with and without the thermal stage and their dependence on the temperature of the thermal stage are also in agreement with the assignment. A higher temperature led to a reduction in the relative intensity of the immobilized component in for both Si/P123 = 59 and 118 preparations. This is consistent with Glarneaue et al.,[13] who reported that hydrothermal treatment reduces the extent of the micropores and when it is carried out at 130 °C they are eliminated almost completely. Indeed, nitrogen absorption isotherms of the samples studied showed a reduction in the degree of microporosity after the 100 °C thermal stage. The microporosity reduction was, however, more pronounced for Si/P123 = 118. This decrease is also manifested in an increase in the *d*-spacing accompanied by the reduction in the silica wall thickness caused by the compression of the silica.

Our results show that under the present reaction conditions, prior to the thermal part of the reaction 77% of the PEO chains of L62-NO are located within the silica network. This suggests that a significant amount of the PEO part of the P123 chains are within the silica. The thermal stage leads to the release or retracting of part of the PEO chains back into the organic core where its motional freedom is high. This is supported by the ^{13}C NMR experiments that showed that the methylene groups of the PEO chains are less mobile and experience an inhomogeneous environment as compared to those of the PPO chains and after the thermal stage the mobility of part of them increased.

Now that the two environments probed by the spin-label in the final products of SBA-15(P123) have been assigned, we proceed to discuss the temporal evolution of the EPR spectrum during synthesis (Figs. 6a), which also shows a partitioning of the spin-label between two environments. While the EPR spectrum of one component remains invariant throughout the reaction, the other exhibits a continuous decrease of a_N during the first 100 min. When the Si/P123 ratio was increased by a factor of 2, the extent of the a_N reduction increased as well. The spin-label in both environments is highly mobile indicating that prior to drying the water content of the silica network is large and the network is highly fluid. Drying has a pronounced effect on the mobility of the PEO chains of L62-NO, showing that most of the water can be easily removed causing a "hardening" of the silica wall. The SBA(L64) synthesis did not reveal any partitioning into two environments, and the spectrum remained practically invariant throughout the reaction. Similarly, the final product showed only a single type of immobilized L62-NO PEO chains.

The question that arises is which of the two environments observed during the synthesis is the precursor of the L62-NO PEO chains trapped within the micropores. The reduction in a_N throughout the reaction shows that one of the environments experiences a continuous reduction in polarity as the silica network is formed. One possibility is that the changing environment corresponds to NO groups that remain within the region of the corona−core interface, and as the silica network is formed, the water content in this region is lowered, and therefore, a_N is reduced too. This is a reasonable situation considering that the PEO chains of L62 are significantly shorter than those of P123 (6 vs 20) and is also consistent with the high mobility of this component after drying because it is rather distant from the silica interface. This also implies that the silica network does not extend all of the way to the corona−core interface. When the Si/P123 ratio is raised, the thickness of the silica network increases, yielding a larger relative amount of micropores and a higher degree of water depletion in the region of L62-NO PEO chains that remain in the corona−core interface. Therefore, we conclude that the invariant environment corresponds to the precursors of the PEO chains trapped in the micropores. According to this model, in SBA(L64), the silica penetrates closer to the core such that the extent of the PEO chains of L62-NO that are trapped within the silica is high because the PEO length of L64 and L62 are closer (6 vs 13) than in P123. Consequently, they do not experience any significant change in the polarity of the environment. Upon drying, the spectrum exhibits a single immobilized species because of the removal of the water and the stronger interaction with the silica, similar to the L62-NO PEO chains trapped in the micropores of SBA-15(P123). The shorter PEO chains in L64 results in a lower degree of microporosity (see Table 1). The increased mobility of the L62-NO PEO chains upon the thermal stage of the SBA(L64) synthesis suggests a reduction in the interaction with the silica surface as a consequence of dehydroxylation resulting in a higher degree of silica condensation. The alternative model where the silica network polarity is reduced as the reaction progresses and finally becomes less polar than the organic part seems unlikely. This would imply that in the L64 case the PEO chains of L62 are all in the organic part, which will make it difficult to explain the rigid limit spectrum observed after drying.

The model depicted in Figure 10 shows a schematic structure of SBA-15(P123) and SBA(L64) prior to the thermal stage, based on our results. The light gray color in Figure 10 represents the silica network, the dark gray color corresponds to the part of the PEO chains in the mesopores, and the white color is the PPO chains region of the mesopores. The black dots symbolize to the NO groups at the end of the L62-NO PEO chains. The thermal stage reduces the extent of the PEO chains in the silica and thereby decreases the silica wall thickness and increases the mesopore diameter. This is manifested in the increase of the dark gray area and the inclusion of more NO groups (black spots) in this region in the case of P123 synthesis.

Conclusions

In aqueous micellar solutions of Pluronics P123, the nitroxide spin-label of L62-NO is located within the micelles close to the corona−core interface, whereas in L64, it is situated closer to the center of the corona. Consequently, it is an excellent candidate for the in situ EPR investigation of the formation mechanism of SBA-15 in general and the initiation of the micropores in particular. We have shown experimentally that the source of the microporosity is the PEO chains that are

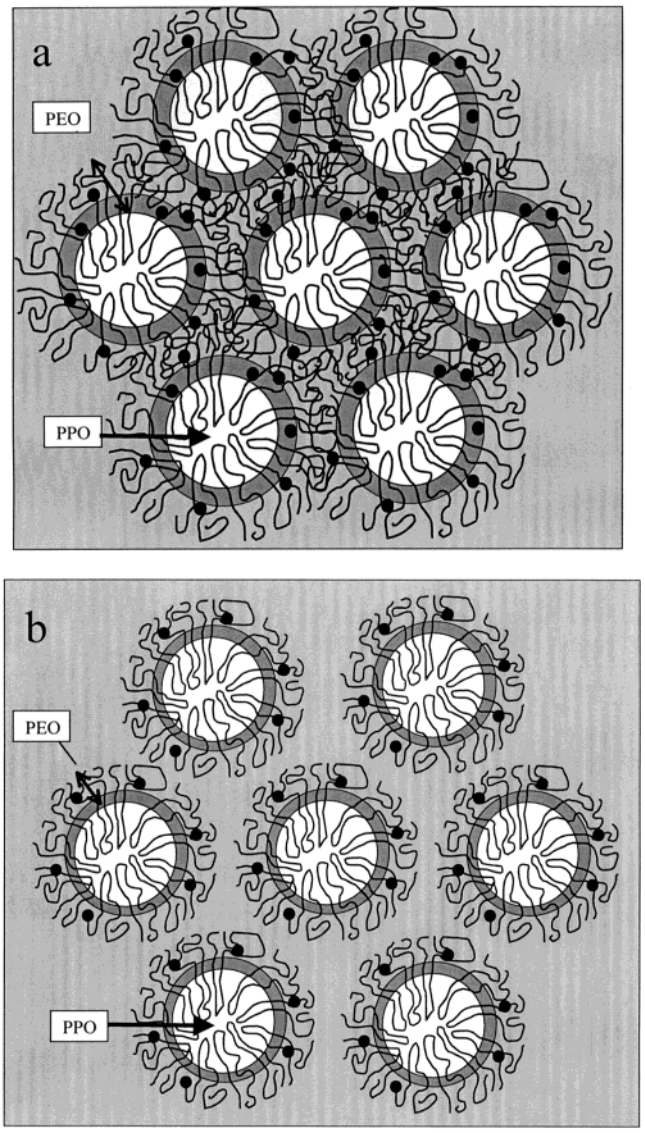

Figure 10. Proposed model for the SBA structures after a reaction at 50 °C before the thermal stage. (a) Synthesized with P123 (b) with L64. The light gray color represents the silica network, the dark gray color corresponds to the part of the PEO chains in the mesopores, and the white color is the PPO chains region of the mesopores. The black dots are the NO groups of L62-NO spin label.

trapped within the silica region. In the first stage of the reaction, a fluid silica network with a high water and PEO content is formed within the first 2 h along with the establishment of the hexagonal order. In the case of the P123 synthesis, a partitioning of the L62-NO spin-probe between the precursors of the mesopores and micropores of the SBA-15 structure takes place at the very early stages of the reaction, and a continuous depletion of the water within the corona−core interface is observed. In the final product obtained without the thermal stage, the majority of the PEO chains are located in the micropores. The extent of the EO chains in the silica depends on the thermal stage temperature and on the Si/P123 molar ratio. In the L64 synthesis, practically all of the NO groups of L62-NO are located within the silica network and experience only one environment.

Acknowledgment. This research was supported by center of excellence "Origin of ordering and functionality in mesostructured hybrid materials." supported by THE ISRAREL SCIENCE FOUNDATION (Grant No. 800301-1) and Minerva Foundation, Germany.

References and Notes

(1) Beck, J. S.; Vartuli, J. C.; Roth, W. J.; Leonowicz, M. E.; Kresge, C. T.; Schmidtt, K. D.; Chu, C. T−W.; Olson, D. H.; Sheppard, E. W.; McCullen, S. B.; Higgins, J. B.; Schlenker, J. L. *J. Am. Chem. Soc.* **1992**, *114*, 10834.

(2) Kresge, C. T.; Leonowicz, M. E.; Roth, W. J.; Vartuli, J. C.; Beck, J. S. *Nature* **1992**, *359*, 710.

(3) Selvam, P.; Bhatia, S. K.; Sonwane, C. G. *Ind. Eng. Chem. Res.* **2001**, *40*, 3237.

(4) Huo, Q.; Leon, R.; Petroff, P. M.; Stucky, G. D. *Science* **1995**, *268*, 1324.

(5) Ying, J. Y.; Mehnert, C. P.; Wong, M. S. *Angew. Chem. Ind. Ed.* **1999**, *38*, 56.

(6) Patarin, J.; Lebeau, B.; Zaba, R. *Curr. Opin. Interface Sci.* **2002**, *7*, 107.

(7) Schüth, F. In *Studies in Surface Science and Catalysis*; Galarneau, A., Di Remzo, F., Fajula, F., Vedrin, J., Eds.; Elsevier: 2001; Vol. 135, p 1.

(8) Zhao, D.; Huo, Q.; Feng, J.; Chmelka, B. F.; Stucky, G. D. *J. Am. Chem. Soc.* **1998**, *120*, 6024.

(9) Huo, Q.; Margolese, D. I.; Ciesla, U., Demuth, D. G.; Feng, P.; Gier, T. E.; Sieger, P.; Firuzi, A.; Chemalka, B. F.; Schuth, F.; Stucky, G. D. *Chem. Mater.* **1994**, *6*, 1176.

(10) Tanev, P. T.; Pinnavaia, T. J. *Science* **1995**, *267*, 865.

(11) Bagashaw, S. A.; Prouzet, E.; Pinnavaia, T. J. *Science* **1995**, *269*, 1242.

(12) Ryoo, R.; Ko, C. H. *J. Phys. Chem. B* **2000**, *104*, 11465.

(13) Galarneau, A.; Cambon, H.; Renzo, F. D.; Fajula, F. *Langmuir* **2001**, *17*, 8328.

(14) Imperor-Clerc, M.; Davidson, P.; Davidson, A. *J. Am. Chem. Soc.* **2000**, *122*, 11925.

(15) Miyazawa, K.; Inagaki, S. *Chem. Commun.* **2000**, 2121.

(16) Voort, P. V. D.; Ravikovitch, P. I.; Jong, K. P. D.; Neimark, A. V.; Janssen, A. H.; Benjelloun, M.; Van Bavel, E.; Cool, P.; Weckhuysen, B. M., Vansant, E. F. *Chem. Commun.* **2002**, 1010.

(17) Kruk, M.; Jaroniec, M.; Ko C. H.; Ryoo, R. *Chem. Mater.* **2000**, *12*, 1961.

(18) Melosh, N. A.; Lipic, P.; Bates, F. S.; Wudel, F.; Stucky, G. D.; Fredrickson, G. H.; Chmelka, B. F. *Macromolecules* **1999**, *32*, 4332.

(19) Zhang, J.; Luz, Z.; Goldfarb, D. *J. Phys. Chem. B* **1997**, *101*, 7087.

(20) Zhang, J.; Luz, Z.; Zimmermann, H.; Goldfarb, D. *J. Phys. Chem. B* **2000**, *104*, 279.

(21) Galarneau, A.; Renzo, F.; Fajula, F.; Mollo, L.; Fubini, B.; Ottaviani, M. F. *J. Colloid. Interface. Sci.* **1998**, *201*, 105.

(22) Caragheorgheopol, A.; Caldararu, H.; Dragutan, I.; Joela, H.; Brown, W. *Langmuir* **1997**, *13*, 6912.

(23) Zhao, D.; Sun, J.; Li, Q.; Stucky, G. D. *Chem. Mater.* **2000**, *12*, 275.

(24) Gromov, I.; Krymov, V.; Manikandan, P.; Arieli, D.; Goldfarb, D. *J. Magn. Reson.* **1999**, *139*, 8.

(25) Shane, J. J.; Gromov, I.; Vega, S.; Goldfarb, D. *Rev. Sci. Instrum.* **1998**, *69*, 3357.

(26) Fauth, J. M.; Schweiger, A.; Braunschweiler, L.; Forrer, J.; Ernst, R. R. *J. Magn. Reson.* **1986**, *66*, 74.

(27) Cheethman, J. J.; Wachtel, E.; Bach, D.; Epand, R. M. *Biochemistry* **1989**, *28*, 8928.

(28) Budil, D. E.; Lee, S.; Saxena, S.; Freed, J. H. *J. Magn. Reson. A* **1996**, *120*, 155.

(29) Schnider, D. J.; Freed, J. H. In *Biological Magnetic Resonance. Spin Labeling*; Berliner, L. J., Reuben, J., Eds.; Plenum: New York, 1989; Vol. 8, Chapter 1.

(30) Ottaviani, M. F.; Daddi, R.; Brustolon, M.; Turro, N. J.; Tomilia, D. A. *Langmuir* **1999**, *15*, 1973.

(31) Morrisett, J. D. *Spin Labeling (Theory and Applications)*; Academic Press: New York, 1976; Chapter 8.

(32) Rozantsev, E. G. *Free Nitroxyl Radicals*; Plenum Press: New York, 1970.

(33) Alexandridis, P.; Hatton, A. T. *Colloids Surf. A: Physicochem. Eng. Aspects* **1995**, *96*, 1.

(34) Wanka, G.; Hoffman, H.; Ulbricht, W. *Macromolecules* **1994**, *27*, 4145.

(35) Schweiger, A.; Jeschke, G. *Principles of Pulse Electron Paramagnetic Resonance*; Oxford University Press: New York, 2001.

(36) Dikanov, S. A.; Tsvetkov, Yu. D. *Electron Spin−Echo Envelope Modulation (ESEEM) Spectroscopy*; CRC Press: Boca Raton, 1992.

(37) Kevan, L. In *Modern Pulsed and Continues Wave Electron Spin*

Rresonance; Kevan, L., Bowman, M. K., Eds.; Wiley: New York, 1990.
(38) Kang, Y. S.; Kevan, L. *J. Phys. Chem.* **1994**, *98*, 7624.
(39) Stenland, C.; Kevan, L. *Langmuir* **1994**, *10*, 1129.
(40) Kursev, V. V.; Kevan, L. *J. Phys. Chem.* **1995**, *99*, 10616.
(41) Baglioni, P.; Rivara-Minten, E.; Kevan, L. *J. Phys. Chem.* **1988**, *92*, 4276.
(42) Baglioni, P.; Kevan, L. *J. Phys. Chem.* **1987**, *91*, 1516.
(43) Hiff, T.; Kevan, L. *J. Phys. Chem.* **1989**, *93*, 1572.
(44) Zhang, J.; Carl, P. J.; Zimmermann, H.; Goldfarb, D. *J. Phys. Chem. B* **2002**, *106*, 5382.
(45) Zhao, D.; Feng, J.; Huo, Q.; Melosh, N.; Fredrickson, G.; Chmelka, B.; Stucky, G. D. *Science* **1998**, *279*, 548.
(46) Caragheorgheopol, A.; Schlick, S. *Macromolecules* **1998**, *31*, 7736.